第 37 卷第 5 期
2018 年 10 月

红 外 与 毫 米 波 学 报
J. Infrared Millim. Waves

Vol. 37, No. 5
October, 2018

文章编号: 1001 - 9014(2018)05 - 0533 - 07

DOI: 10.11972/j.issn.1001 - 9014.2018.05.005

Enhance absorption based on the resonance of localized surface plasmon modes in a metamaterial absorber

ZHANG Zhen-Ya[1,2,3], LIU Xiao-Li[2*], WEN Xiao-Dong[1,3*]

(1. School of Architecture and Transportation Engineering, Ningbo University of Technology, Ningbo 315211, China;
2. State key Laboratory of Hydroscience and Engineering, Tsinghua University, Beijing 100084, China;
3. School of electrical information engineering, Yunnan Minzu University, Kunming 650031, China)

Abstract: In this paper, we present a single peak absorption characteristic of high performance metamaterial absorber in 150 ~ 165 THz region. The designed absorber contains two arrays: a dual metallic particles array and a dual air holes array. The damping constant of metal layer is optimized in simulations. It is found that the maximum absorption rate 96% can be obtained when using 2.3 times of damping constant in simulations. The absorption peak is excited by the localized surface plasmon (LSP) modes resonance. In order to reveal the resonant electromagnetic mechanism and research the effects of structural parameters variations on the resonant absorption peak, two sets of simulations were carried out. It was found that with increasing the vertical distance V, the absorption peak is enhanced and a new absorption band is achieved when V = 160 nm. In the second simulations, for the increase in horizontal distance H, the absorption peak is also enhanced and another new absorption band is achieved when H = 190 nm. Electric field intensity distribution results show the excitation of LSP modes and the coupling effect between LSP modes lead to the absorption peak enhanced phenomenon.

Key words: metamaterials, absorption peaks, metal particles
PACS: 41.20.Jb, 78.20.Cj, 73.20.Mf

基于局部表面等离子体激元的共振增强超材料吸收器的吸收性质

张振亚[1,2,3], 刘晓丽[2*], 温小栋[1,3*]

(1. 宁波工程学院建筑与交通工程学院, 浙江 宁波 315211;
2. 清华大学水沙科学与水利工程国家重点实验室, 北京 100084;
3. 云南民族大学电子信息工程学院, 云南 昆明 650031)

摘要: 提出了一种在 150 ~ 165 THz 区域内的具有单峰吸收特性的高性能超材料吸收器。设计的吸波器包含两个阵列: 双金属颗粒阵列和双空气孔阵列。金属层的阻尼常数在模拟中被优化。发现在模拟中使用 2.3 倍的阻尼常数时, 可以获得最大吸收率 96%。吸收峰由局域表面等离子体(LSP)模式共振激发。为了揭示共振电磁机理, 进行了两组模拟, 研究结构参数变化对共振吸收峰的影响。发现随着垂直距离 V 的增加, 吸收峰被增强, 当 V = 160 nm 时, 获得新的吸收带。在第二次模拟中, 对于水平距离 H 的增加, 吸收峰也增强, 并且当 H = 190 nm 时获得另一个新的吸收带。电场强度分布结果表明 LSP 模式的激发和 LSP 模式之间的耦合效应导致吸收峰增强现象。

关 键 词: 超材料; 吸收峰; 金属颗粒

中图分类号: O43 **文献标识码:** *A*

Received date: 2017-10-25, **revised date:** 2018-04-09 **收稿日期:** 2017-10-25, **修回日期:** 2018-04-09

Foundation items: Supported by the Public Welfare Technology Research Project of Zhejiang Province (2014C31042), National Natural Science Foundation of China (51569035), the Natural Science Foundation of Zhejiang province, China (LY15E080014), preparatory funds of School of Architecture and Transportation, Ningbo university of technology, Open Research Fund Program of State key Laboratory of Hydroscience and Engineering

Biography: ZHANG Zhen-Ya (1978-), male, Shandong. Research area involves: Dynamics of materials and structures, design and preparation of metamaterials. E-mail: lttpff@163.com

* **Corresponding author:** xiaoli.liu@tsinghua.edu.cn, wenxiaodong8@163.com

Introduction

Metamaterials is an artificially designed and manufactured electromagnetic resonance material, which shows many unique properties [1-4]. The manufacture and industrial development of metamaterial attracted the attention of researchers [5-7]. The existing simulation results and experimental results show that metamaterials can be applied in many fields, including thermal emitters, metamaterial absorbers, sensors, photodetectors, photovoltaic cells, and optical imaging devices [8-13]. On the one hand, many novel structural design strategies have been proposed and validated [14-17]. For the metallic holes structure design strategy, *Ebbesen et al* revealed the property of the extraordinary optical transmission (EOT) phenomenon in a metallic holes structure metamaterial [18]. It is generally believed that the EOT phenomenon is due to the resonance of surface plasmon polaritons (SPP) mode on metal film and the localized surface plasmon (LSP) mode of individual holes structure [19]. The LSP mode is related to the resonance of Fabry-Pérot-like mode in individual hole [20]. For the metallic particles structure design strategy, it was confirmed that the LSP mode resonance can be support by metallic particle structure metamaterial [21]. The LSP mode resonance is sensitive to the local dielectric materials, shape, size, material of particles [22-25]. Such plasmon resonance can be applied in many fields [26-27]. *García de Abajo* indicated that the LSP mode resonance can be supported by both the metallic particles and hole arrays [28]. On the other hand, many novel metallic particles and holes structure design strategies are applied in developing of metamaterial absorbers. A variety of typical metamaterial absorber structures were reported [29-34]. For the pure metal particles structure metamaterial absorber, Nan Zhang *et al* [35] designed and experimentally verified a dual-band metamaterial absorber based on the dielectric and ohmic loss. The proposed metamaterial absorber showed high absorption property with different dielectric spacing layers. For the pure metal hole structure metamaterial absorber, Prakash Pitchappa *et al.* [36] designed and experimentally verified a dual-band metamaterial absorber in the near infrared region, which was based on the electrical resonance and the cavity resonance. The designed metamaterial absorber revealed high absorption property based on optimizing the hole dimension and the spacer thickness. Moreover, the proposed metamaterial absorber could be modulated from dual-band to single-band based on the coupling effect between the electrical resonance and cavity resonance. With the development of science and technology, a kind of composite structure metamaterial absorber is proposed, for example, Withawat Withayachumnankul *et al.* [37] proposed and manufactured a perfect metamaterial absorber in the terahertz region, which is based on the coupling between the cavity mode and coaxial surface plasmon polaritons. The designed composite structure is composed of concentric metal holes and metal particles. However, few literatures report the effect of the interaction of LSP modes between particles and holes array on absorption. In this paper, a composite structure absorber with metallic particles array and holes array is designed and simulated. It is found that the pure dual metallic holes structure can achieve an absorption peak (58%) at 155 THz, while the pure dual metallic particles can achieve two absorption peaks (35%, 32%) at 157 THz and 159 THz. It is dramatic that a near perfect absorption peak (96%) can be achieved at 154.2 THz when these pure structures are combined into the proposed composite structure in this paper. The near perfect absorption peak is excited by the coupling of LSP modes, which can't be found in these pure structures. The horizontal or vertical distances between two metallic particles are optimized in two set of simulations. It is found that the property of the absorber is directly affected by the horizontal or vertical distances. Moreover, new absorption bands can be obtained due to the enhanced coupling of LSP modes on edges of metallic holes.

1 Structural design and theoretical model

1.1 Structural design

The designed composite structure metamaterial absorber is shown in Figs. 1(a-b). The designed structure consists of three functional layers: the bottom layer is a completely gold layer, which works as an eliminator. The intermediate medium layer is MgF_2. The top layer is a patterned gold layer with a dual gold particles array and a dual gold holes array. In the proposed structure, the lattice constant is set as "P", the thickness of gold layer is given by "h1", the thickness of MgF_2 layer is set as "h2", and the diameter of the gold particle and hole are "D1" and "D2". Detailed dimensional parameters are shown in Table 1. In this paper, two structural parameters are defined: the vertical distance (V) is the distance between two gold particles along the Y axis, and the horizontal distance (H) is the distance between two gold particles along the X axis. The thickness of the gold layer is 155 nm and the MgF_2 layer is 400 nm. The thickness of the air layers above and below the absorber are 1 500 nm and 500 nm, respectively. The software Ansofts HFSS 10.0 is used in simulations. Gold layer follows the Drude model with the is the plasma frequency, while the is the collision frequency [38]. Due to the bottom gold layer is thick enough; the simulated transmission closes to zero in simulations. Therefore, the simulated absorption is given by:

$$A(f) = 1 - R(f) \quad . \quad (1)$$

In our simulations, the electromagnetic properties of the MgF_2 layer follow the results of reference [39]. Ideal electric and conductor planes are applied on boundaries of the unite cell [40]. The whole unite cell is simulated in air with electromagnetic wave incident from air along the -z axis.

Table 1 Detailed dimensional parameters
表1 详细的结构参数

Parameter	P	$D1$	$D2$	$h1$	$h2$	w
Value/nm	900	90	400	155	400	40

1.2 Optimization of metal layer parameters

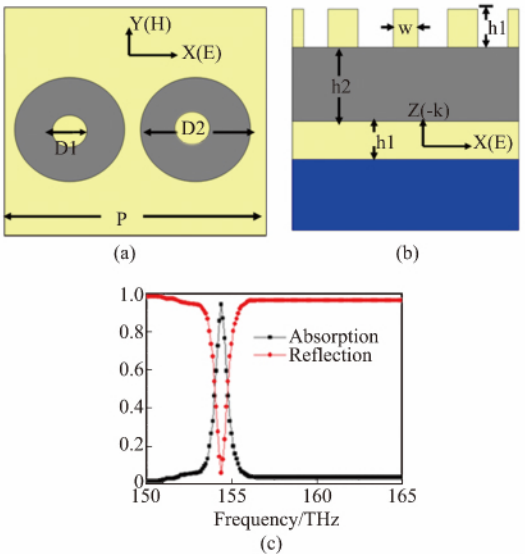

Fig. 1　(a) Top view of the proposed unit cell, (b) Cross section view (The yellow part is gold layer, the gray part is MgF_2 layer, and the blue part is the glass substrate), (c) Simulated absorption and reflection spectra

图 1　(a) 结构设计的俯视图,(b) 结构设计的横截面图,(c) 吸收谱和反射普的仿真结果. 黄色部分是金属层,灰色部分是氟化镁,蓝色部分是玻璃基板

Zhang, *et al.* indicated that the damping constant of gold layer in simulations maybe lower than that of the bulk gold layer in the real system. This is because the grain boundary effect and the surface scattering effect on the property of gold layer [41]. Moreover, Liu *et al.* [42] achieved a perfect absorption rate through optimizing the damping constant of the Drude model in simulations. The 3.0 times of the damping constant was adopted in simulations based on the results in literature [41]. Therefore, the influence of the damping constant on the absorption performance should be seriously treated before revealing the electromagnetic properties of the proposed memamaterial absorber. According to the basic methods of literature [41-42], the gold layer parameter of the proposed unite cell is also optimized in this paper. In order to clear the impact of the damping constant on the absorption performance of the designed memamaterial absorber, Fig. 2 shows the simulated absorption spectra for damping constants of 1.0, 2.3, and 3.6 times in simulations. It is found that the maximum absorption rate reaches 76% for one time of damping constants, as shown in Fig. 2. For the adopted damping constant equal to 2.3 times that of bulk gold, the maximum absorption rate increases to 96%, as shown in Fig. 1(c) and Fig. 2. However, for the 3.6 times of damping constants, the maximum absorption rate reduces to 85%. A strong resonance with nearly 100% absorption is achieved for 2.3 times damping constant of bulk gold. Consequently, a perfect metamaterial absorber is obtained with 2.3 times damping constant of bulk gold. In the following simulations, the damping constants of bulk gold layers are all used 2.3 times damping constant.

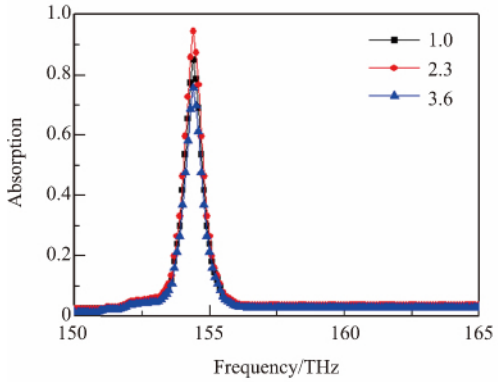

Fig. 2　Simulated absorption spectrum with different times of damping constant of bulk gold

图 2　在不同阻尼常数金属层条件下得到的仿真吸收谱

2　Results and discussion

2.1　Physical mechanism

The simulated absorption spectrum of two pure structures are calculated, as shown in Fig. 3. It is found that, for the pure dual metallic holes structure, an absorption peak is obtained at 155 THz, as shown in Fig. 3. For pure the dual metallic particles structure, two absorption peaks are obtained at 157 THz and 159 THz. The maximum absorption rates of two pure structures are lower than that of the proposed unite cell. To reveal the physical mechanism of the proposed unite cell, the electric field distributions are calculated. The calculated electric field distributions is a method often used to describe the electromagnetic resonance behaviors of metamaterial absorbers [43-44]. Moreover, the electric field distributions of pure structures are also calculated, as shown in Fig. 4. For the dual metallic holes unite cell, a LSP mode is effectively excited on the edge of one hole, as shown in Fig. 4(a), which leads to the absorption peak at 155 THz in Fig. 3. For the dual metallic particles unite cell, two resonance frequencies are selected in simulations. At 157 THz, LSP modes are excited on edges of one metallic particle, as shown in Fig. 4(b). And at 159 THz, two LSP modes are excited on edges of another metallic particle, as shown in Fig. 4(c). The resonance intensity of LSP modes in dual metallic particles unite cell is weaker than that in the dual metallic holes unite cell, which results in the difference in maximum absorbance rates. However, for the proposed unite cell, the strong LSP modes resonance can be found obviously, which leads to the absorption peak at 154.2 THz in Fig. 3. It is found that the resonance intensity of LSP modes plays an important role in absorption peak rate. In order to characterize the electromagnetic properties of the proposed metamaterial absorber, the S parameters retrieval method [45-46] is used to retrieve the effective parameters (effective permeability μ, permittivity ε, and impedance Z), as shown in Fig. 5. The effective permeability μ and permittivity ε can be obtained as following [47]:

$$\mu(f) = \mu_0\left(1 - \frac{Ff_e^2}{f^2 - f_m^2 - j\gamma_m f_m}\right) \quad , \quad (2)$$

$$\varepsilon(f) = \varepsilon_0\left(\varepsilon_\infty - \frac{f_e^2}{f^2 - j\gamma_e / f}\right) \quad . \quad (3)$$

Here, f is the simulation scan frequency, F is the filling factor, γ_m and γ_e are damping factors, f_m is the frequency associated with the magnetic resonance [48]. It can be found that the real parts of the effective permeability μ and permittivity ε are equal to each other at the resonance frequency of the absorption peak. Therefore, the effective impedance can be achieved as following [47]:

$$Z(f) = \sqrt{\mu(f)/\varepsilon(f)} \approx Z_0 = 1 \quad . \quad (4)$$

Here, the effective impedance Z of the proposed absorber is near to the free space, which results in the high absorption peak in Fig. 3. The imaginary parts of the effective parameters are also calculated, as shown in Fig. 5. It is obviously that the imaginary parts of the effective permeability μ and permittivity ε are maximized at the resonance frequency of the absorption peak, which implies the metamaterial has high absorption loss [49]. Moreover, the the imaginary parts of the effective impedance Z is closed to zero, which implies low reflection loss. These electromagnetic resonance behaviors result in the absorption peak [50].

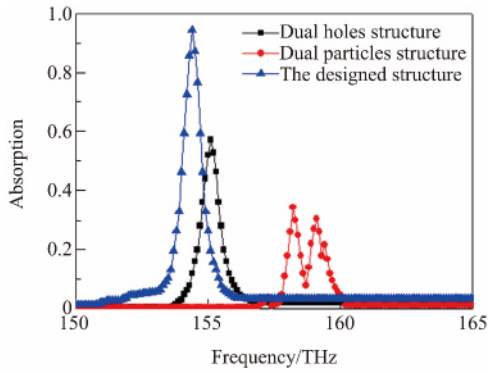

Fig. 3 The absorption spectrum of pure dual holes structure array, pure dual particles structure array, and the designed structure

图3 单独的双孔阵列结构的仿真吸收谱,单独的双金属颗粒阵列结构的仿真吸收谱,以及本文设计的结构的仿真吸收谱

2.2 Vertical distance optimization

The effect of the vertical distance (V) along the y axis on the absorption rate is revealed in the first set of simulations. Fig. 6 shows the absorption spectrum with different V between two metallic particles, while other structural parameters unchanged. When V = 80 nm, the maximum absorption peak is 93%, and the bandwidth is increased, see the red curve in Fig. 6. Two new absorption peaks are obtained at 153.6 THz and 154.9 THz. When V = 160nm, the maximum absorption rate is 95%. Moreover, a broad absorption band is obtained, see the blue curve in Fig. 6. However, for the V = 220 nm, the maximum absorption rate is abnormally reduced, see the green curve in Fig. 6. To survey the electromagnetic resonance behavior behinds the absorption spectrum

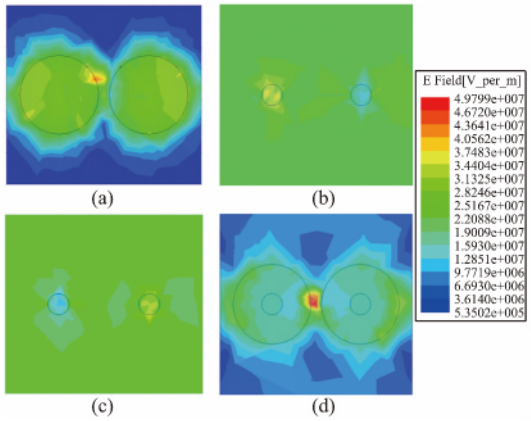

Fig. 4 Simulated electric field in the X-Y plane illuminated under normally incident wave with different resonance frequencies, (a) 155 THz, (b) 157 THz, (c) 159 THz, (d) 154.2 THz

图4 在电磁波垂直入射条件下不同共振频率的仿真电场分布,(a) 155 THz, (b) 157 THz, (c) 159 THz, (d) 154.2 THz

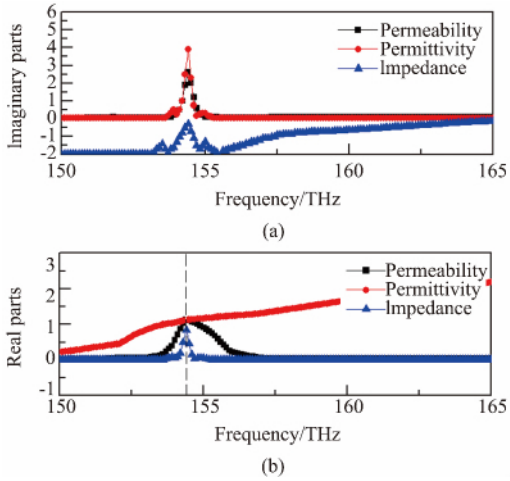

Fig. 5 (a) The imaginary parts of the effective parameters (effective permeability μ, permittivity ε, and impedance Z), (b) the real parts of the effective parameters (effective permeability μ, permittivity ε, and impedance Z)

图5 (a) 有效参数(有效磁导率,介电常数和阻抗)的虚部,(b) 有效参数(有效磁导率,介电常数和阻抗)的实部

in Fig. 6, the electric field distributions are calculated, as shown in Fig. 7. Four resonance frequencies of the absorption peak are selected in simulations. LSP modes between edges of two metallic holes are effectively excited, which leads to the absorption peak. When the V is increased, two new LSP modes are excited on edges of two metallic holes. The original LSP modes and two new LSP modes are excited at the resonance frequency 155 THz. Moreover, two new LSP modes coupling with original LSP modes, which results in the absorption peak expanding (see the red curve in Fig. 6), as shown in Fig.

7 (b) . These simulated results indicate that the new LSP modes resonance and the coupled effect between LSP modes play an important in enhancing the absorption performance. When V = 160 nm, the resonance intensity of all LSP modes is became higher. At the same time, the coupled effect between LSP modes is also increased. An absorption band is revealed by these enhanced resonance behaviors (see the blue curve in Fig. 6) , as shown in Fig. 7(c) . When V = 220 nm, two metallic particles touch with two metallic holes, a new gold layer is obtained. However, these LSP modes can't be effectively excited [49] , which leads to the absorption band disappear and the absorption rate reduce in Fig. 6. To real the electromagnetic properties of the absorption band in Fig. 6, the real parts of the effective parameters are retrieved by the S parameters retrieval method, as shown in Fig. 8. It can be found that the real part of the effective permeability μ and permittivity ε show more intense resonance behaviors than that in Fig. 5 with the vertical distance increasing. These strong electromagnetic resonance behaviors cause the slope of the real part of the permeability μ and permittivity ε is the same (V = 160 nm, see the area between the two dotted lines in Fig. 8) , which results in the near perfect impedance matching [47] in Fig. 8 and the absorption band in Fig. 6. The imaginary parts of the effective parameters are shown in Fig. 8, too. The imaginary parts of the effective permeability μ and permittivity ε are maximized in the absorption band. At the same time, the imaginary parts of the effective impedance Z is closed to zero. These electromagnetic resonance behaviors result in the absorption band.

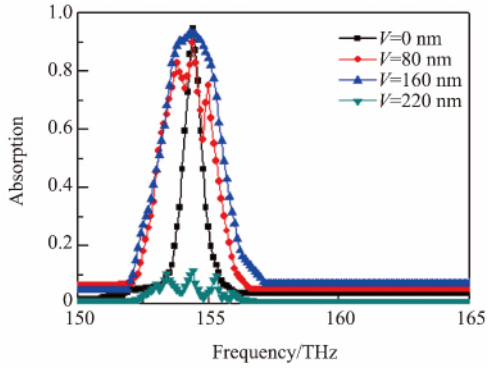

Fig. 6　The simulated absorption spectrum with different vertical distances

图 6　不同垂直距离条件下的仿真吸收谱

2.3　Horizontal distance optimization

The second set of simulations is carried out to investigate the effect of the horizontal distance (H) along the x axis on the absorption property. Figure 9 shows the absorption spectrum with different H, while other structural parameters unchanged (V = 0 nm) . When the H = 310 nm, two metallic particles close to each other, the maximum absorption rate is 91%, see the red curve in Fig. 9. Two new absorption peaks are obtained at 153.8 THz and 154.7 THz. When two metallic particles continue to approach (H = 190 nm) , a new absorption band is obtained, as shown in Fig. 9. Similarly, when H = 130 nm, two metallic particles touch with two metallic holes,

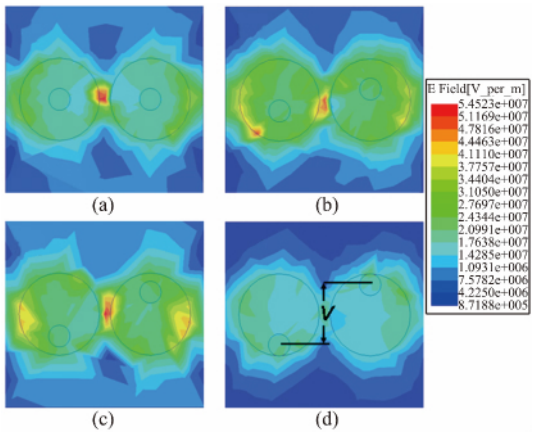

Fig. 7　Simulated electric field intensity distributions with different vertical distances (V = 0 nm, 80 nm, 160 nm, and 220 nm) , H = 440 nm

图 7　不同垂直距离条件下的仿真电场分布 (V = 0 nm, 80 nm, 160 nm, and 220 nm) , H = 440 nm

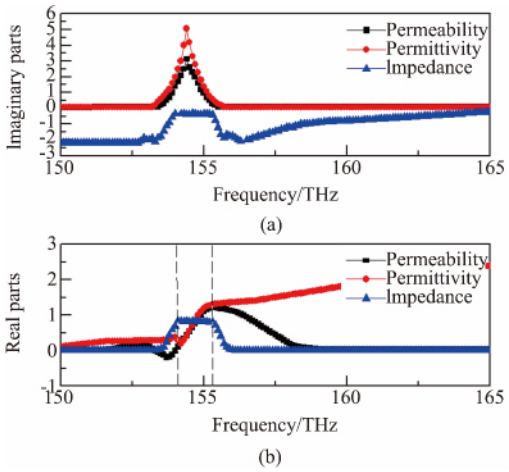

Fig. 8　(a) The imaginary parts of the effective parameters (effective permeability μ, permittivity ε, and impedance) (V = 160 nm) . (b) The real parts of the effective parameters (effective permeability μ, permittivity ε, and impedance Z) (V = 160 nm)

图 8　(a) 有效参数(有效磁导率,介电常数和阻抗) 的虚部(V = 160 nm) . (b) 有效参数(有效磁导率,介电常数和阻抗) 的实部(V = 160 nm)

the absorption band disappear and the absorption is abnormally decreased. The corresponding electric field distributions are calculated, as shown in Fig. 10. When two metallic particles close to each other (H = 310 nm) , two new LSP modes are also excited on edges of two metallic holes, as shown in Fig. 10(b) , which is similar to the above. The resonance intensity of these LSP modes is higher than that when H = 190 nm, as shown in Fig. 10 (c) . When H = 130 nm, two metallic particles and the top metal thin form a new metal plate. Moreover, a very weak LSP mode is obtained, which leads to the lower absorption in Fig. 9. Figure 11 shows the real parts of the effective parameters. It is obviously that real part of the effective permeability μ and permittivity ε show stronger resonance behaviors (H = 190 nm, see the area between

the two dotted lines in Fig. 11) in the absorption band with the horizontal distance reducing. The impedance matching condition is also obtained in the absorption band [17], as shown in Fig. 11. The imaginary parts of the effective parameters are also displayed in Fig. 11. The high absorption loss is also achieved in the absorption band because the imaginary parts of the effective permeability μ and permittivity ε are maximized in the absorption band. Moreover, the low reflection loss is obtained. A strong resonance absorption band is achieved according to Eq. 1. The results of the Figs. 5, 8, and 11 indicate that the vertical distances V and the horizontal distance H play an important role on the electromagnetic resonance properties of the proposed absorber. Moreover, the resonance intensity of LSP modes is also directly impacted by the vertical distances V or the horizontal distance H. Therefore, high performance absorber can be achieved by the strong LSP mode resonance behavior.

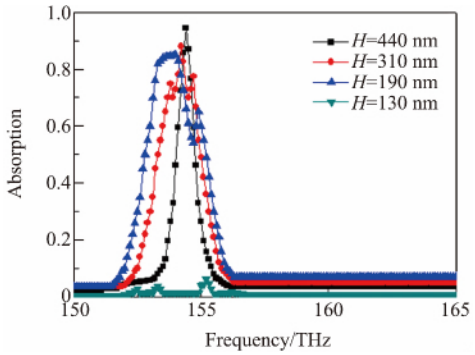

Fig. 9 Simulated absorption spectrum with different horizontal distances

图9 不同水平距离条件下的仿真吸收谱

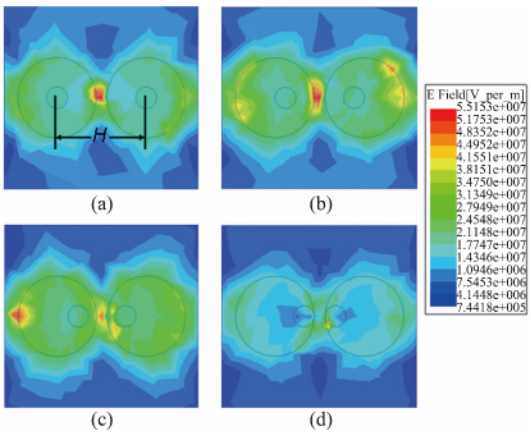

Fig. 10 Simulated electric field intensity distributions with different horizontal distances (H = 440 nm, 310 nm, 190 nm, and 130 nm), V = 0 nm

图10 不同水平距离条件下的仿真电场分布(H = 440 nm, 310 nm, 190 nm, and 130 nm), V = 0 nm

3 Conclusion

In conclusion, we have numerically demonstrated a high performance composite structure metamaterial absorber, which contains a dual metallic particles array and a dual air holes array. In order to obtain accurate absorption performance, the damping constant of metal layer is optimized in simulations. Simulated results indicate that the maximum absorption rate 96% can be obtained when using 2.3 times of damping constant. The physical mechanism of the absorption peak is the LSP modes resonance. Specifically, the vertical distance and horizontal distance between two metallic particles are optimized in simulations. The absorption peak is increased and new absorption bands are obtained due to the coupled effect between LSP modes.

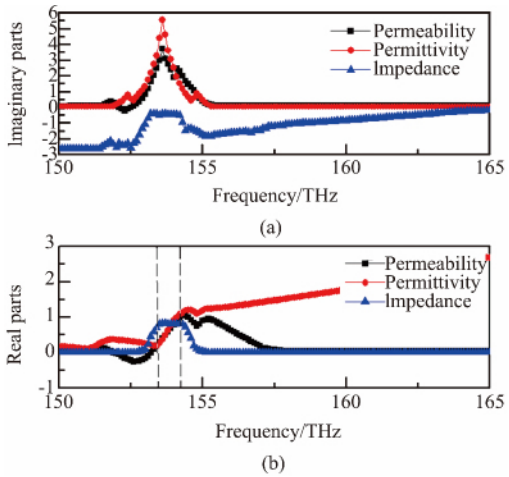

Fig. 11 (a) The imaginary parts of the effective parameters (effective permeability, permittivity μ, and impedance ε) (H = 190 nm), (b) the real parts of the effective parameters (effective permeability μ, permittivity ε, and impedance Z) (H = 190 nm)

图11 (a)有效参数(有效磁导率,介电常数和阻抗)的虚部(H = 190 nm),(b)有效参数(有效磁导率,介电常数和阻抗)的实部(H = 190 nm)

References

[1] Cai W, Chettiar U K, Kildishev A V, *et al*. Optical cloaking with metamaterials [J]. *Nature Photonics* 2007, **1**: 224-227.

[2] Engheta N, Alù A. Plasmonic materials in transparency and cloaking problems: mechanism, robustness, and physical insights [J]. *Optics Express*, 2007, **15**(6): 3318-3332.

[3] Lim S, Caloz C, Itoh T. Metamaterial-based electronically controlled transmission-line structure as a novel leaky-wave antenna with tunable radiation angle and beamwidth [J]. *IEEE Transactions On Microwave Theory And Techniques*, 2004, **52**(12): 2678-2690.

[4] Schurig D, Mock J J, Justice B J, *et al*. Metamaterial electromagnetic cloak at microwave frequencies [J]. *Science*, 2006. **314**: 977-980.

[5] Popov E, Tsonev L, Maystre D, Losses of plasmon surface wave on metallic grating [J]. *J. Mod. Opt*, 1990, **37**: 379-387.

[6] Popov, Maystre D, McPhedran R C, *et al*. Total absorption of unpolarized light by crossed gratings [J]. *Opt. Express*, 2008, **16**: 6146-6155.

[7] Teperik T V, García de Abajo F J, Borisov A G, *et al*. Omnidirectional absorption in nanostructured metal surfaces, *Nat. Photonics*, 2008, **2**: 299-301.

[8] Hu H, Ma C, Liu Z, Plasmonic dark field microscopy [J]. *Appl. Phys. Lett*, 2010, **96**: 113107-113109.

[9] Hao Q, Juluri B K, Zheng Y B, *et al*, Effects of intrinsic fano interference on surface enhanced raman spectroscopy: comparison between

platinum and gold [J]. *J. Phys. Chem. C*, 2010, **114**(42): 18059-18066.
[10] Xiao S, Chettiar U K, Kildishev A V, *et al*, Tunable magnetic response of metamaterials [J]. *Appl. Phys. Lett*, 2009, **95**: 033115-033115.
[11] Munday J N, Atwater H A, Large Integrated Absorption Enhancement in Plasmonic Solar Cells by Combining Metallic Gratings and Antireflection Coatings [J], *Nano Lett*, 2011, **11**: 2195-2201.
[12] Diem M, Koschny T, Soukoulis C M, Wide-angle perfect absorber/thermal emitter in the terahertz regime [J]. *Phys. Rev. B*, 2009, **79**: 033101-033104.
[13] Rosenberg J, Shenoi R V, Vandervelde T E, *et al*, A multispectral and polarization-selective surface-plasmon resonant midinfrared detector [J]. *Appl. Phys. Lett*, 2009, **95**: 161101-161103.
[14] Haes A J, Van Duyne R P, A Nanoscale Optical Biosensor: Sensitivity and Selectivity of an Approach Based on the Localized Surface Plasmon Resonance Spectroscopy of Triangular Silver Nanoparticles [J]. *J. Am. Chem. Soc*, 2002, **124**: 10596-10604.
[15] Hou B, Hang Z H, Wen W, *et al*, Microwave transmission through metallic hole arrays: Surface electric field measurements [J]. *Appl. Phys. Lett*, 2006, **89**: 131917-131919.
[16] Manjavacas A, García de Abajo F J, Robust Plasmon Waveguides in Strongly Interacting Nanowire Arrays [J]. *Nano Lett*, 2009, **9**: 1285-1288.
[17] Fang X, Li Z, Long Y, H. *et al*, Surface-Plasmon-Polariton Assisted Diffraction in Periodic Subwavelength Holes of Metal Films with Reduced Interplane Coupling [J]. *Phys. Rev. Lett*, 2007, **99**: 066805-066812.
[18] Ebbesen T W, Lezec H J, Ghaemi H F, *et al*, Extraordinary optical transmission through sub-wavelength hole arrays [J]. *Nature*, 1998, **391**: 667-669.
[19] Degiron A, Ebbesen T W, The role of localized surface plasmon modes in the enhanced transmission of periodic subwavelength apertures [J]. *J. Opt. A, Pure Appl. Opt*, 2005, **7**: S90-S96.
[20] Yakakura Y, Optical Resonance in a Narrow Slit in a Thick Metallic Screen, Phys. *Rev. Lett*, 2001, **86**: 5601-5604.
[21] Kreibig U, Vollmer M, Optical Properties of Metal Clusters, Springer Series in Material Science [J]. *Springer-Verlag, Berlin*, 1995, **25**: 187-201.
[22] Murray W A, Suckling J R, Barnes W L, Overlayers on Silver Nanotriangles: Field Confinement and Spectral Position of Localized Surface Plasmon Resonances [J]. *Nano Lett*, 2006, **6**: 1772-1777.
[23] Auguié B, Barnes W L, Collective Resonances in Gold Nanoparticle Arrays [J]. *Phys. Rev. Lett*, 2008, **101**: 43902-143904.
[24] Lance Kelly K, Coronado E, Zhao L L, *et al*, The Optical Properties of Metal Nanoparticles: The Influence of Size, Shape, and Dielectric Environment [J]. *The Journal of Physical Chemistry B*, 2003, **107**: 668-677.
[25] Chu Y, Schonbrun E, Yang T, *et al*, Experimental observation of narrow surface plasmon resonances in gold nanoparticle arrays [J]. *Appl. Phys. Lett*. 2008, **93**: 181108-181112.
[26] Beruete M, Sorolla M, Navarro-Cía M, *et al*, Extraordinary transmission and left-handed propagation in miniaturized stacks of doubly periodic subwavelength hole arrays [J]. *Opt. Express*, 2007, **15**: 1107-1114.
[27] García-Vidal F J, Moreno E, J Porto J A, *et al*, Transmission of Light through a Single Rectangular Hole [J]. Phys. Rev. Lett. 2003, **95**: 103901-103903.
[28] García de Abajo F J, Light scattering by particle and hole arrays [J], *Rev. Mod. Phys*. 2007, **79**: 1267-1293.
[29] Liu X L, Tyler T, Starr T, *et al*, Taming the Blackbody with Infrared Metamaterials as Selective Thermal Emitters [J]. *PRL*, 2011, **107**: 045901-045904.
[30] Chen H T, Interference theory of metamaterial perfect absorbers [J]. *OPTICS EXPRESS*, 2012. **20**: 7165-7172.
[31] Liu X L, Starr T, Anthony F. Starr, *et al*, Infrared Spatial and Frequency Selective Metamaterial with Near-Unity Absorbance [J]. *PRL*, 2010, **104**: 207403-207406.
[32] Hao J M, Zhou L, Qiu M, Nearly total absorption of light and heat generation by plasmonic metamaterials [J]. *PHYSICAL REVIEW B*, 2011, **83**: 165107-165118.
[33] Hu C G, Liu L Y, Zhao Z Y, *et al*, Mixed plasmons coupling for expanding the bandwidth of near-perfect absorption at visible frequencies [J]. *OPTICS EXPRESS*, 2009. **17**: 16745-16749.
[34] Zahyun Ku, Brueck S R J, Experimental demonstration of sidewall angle induced bianisotropy in multiple layer negative index metamaterials [J]. *Applied Physics Letters*, 2009, **94**: 153107-153109.
[35] Zhang N, Zhou P H, Cheng D M, *et al*, Dual-band absorption of mid-infrared metamaterialabsorber based on distinct dielectric spacing layers [J]. *OPTICS LETTERS*, 2013. **38**: 1125-1127.
[36] Prakash P, Chong P H, Piotr K, *et al*, Dual band complementary metamaterial absorber in near infrared region [J]. *JOURNAL OF APPLIED PHYSICS*, 2014, **115**: 193109-193114.
[37] Withawat W, Charan M S, Christophe F, *et al*, Plasmonic Resonance toward Terahertz Perfect Absorbers [J]. *ACS Photonics*, 2014, **1**: 625-630.
[38] Ordal M A, Long L L, Bell R J, *et al*, Optical properties of the metals Al, Co, Cu, Au, Fe, Pb, Ni, Pd, Pt, Ag, Ti, and W in the infrared and far infrared [J], *Appl. Opt*. 1983, **22**: 1099-119.
[39] Dodge M J, Refractive properties of magnesium fluoride [J]. *Appl. Opt*. 1984, **23**: 1980-1985.
[40] Smith D R, Schultz S, Markos P, *et al*, Determination of effective permittivity and permeability of metamaterials from reflection and transmission coefficients [J]. *Phys. Rev. B*, 2002, **65**: 95104-195110.
[41] Zhang S, Fan W, Malloy K J, *et al*, Demonstration of metal-dielectric negative-index metamaterials with improved performance at optical frequencies [J]. *J. Opt. Soc. Am. B*, 2006, **23**: 434-438.
[42] Liu N, Martin M, Thomas W, *et al*, Infrared Perfect Absorber and Its Application As Plasmonic Sensor [J]. *Nano Lett*. 2010, **10**: 2342-2348.
[43] Hu C G, Liu L Y, Zhao Z Y, *et al*, Mixed plasmons coupling for expanding the bandwidth of near-perfect absorption at visible frequencies [J]. *OPTICS EXPRESS*, 2009, **17**: 16745-16749.
[44] James G, Yong M, Saha S, *et al*, Polarization insensitive, broadband terahertz metamaterial absorber [J]. *OPTICS LETTERS*, 2011, **36**: 3476-3478.
[45] Mary A, Rodrigo S G, Garcia-Vida F G, *et al*, Theory of negative-refractive-index response of double-fishnet structures [J]. *Phys. Rev. Lett*. 2008, **101**: 103902-103905.
[46] Smith D R, Vier D C, Koschny T, *et al*, Electromagnetic parameter retrieval from inhomogeneous metamaterials [J]. *Phys. Rev. E*, 2005, **71**: 036617-036627.
[47] Jiang Z H, Seokho Y, Lan L, *et al*, Tailoring Dispersion for Broadband Low-loss Optical Metamaterials Using Deep-subwavelength Inclusions [J]. *SCIENTIFIC REPORTS*, 2013, **3**: 1571-1579.
[48] Oughstun, K. E., Shen, S. Dispersive pulse propagation in a double-resonance Lorentz medium [J]. *J. Opt. Soc. Am. B*, 1988, **5**: 2395-2398.
[48] Zhong M, Localized surface plasmon resonnance induced terahertz broad absorption band [J]. *Optics Communications*, 2015, **356**: 607-611.
[49] Jiang Z H, Seokho Y, Lan L, *et al*, Tailoring Dispersion for Broadband Low-loss Optical Metamaterials Using Deep-subwavelength Inclusions [J]. *SCIENTIFIC REPORTS*, 2013, **3**: 1571-1579.
[50] Hao J M, Zhou L, Qiu M, Nearly total absorption of light and heat generation by plasmonic metamaterials [J]. *PHYSICAL REVIEW B*, 2011, **83**: 165107-165110.